A snake robot with a contact force measurement system for obstacle-aided locomotion

Pål Liljebäck, Kristin Y. Pettersen, and Øyvind Stavdahl

***Abstract*— A snake robot can traverse cluttered and irregular environments by using irregularities around its body as push-points to aid the propulsion. This is denoted *obstacle-aided locomotion* and requires the snake robot to have two features: 1) a smooth exterior surface combined with 2) a contact force sensing system. These two features are characteristic of biological snakes, but have received limited attention in snake robot designs so far. This paper describes the development of a new snake robot aimed at meeting both these requirements. The paper details the design and implementation of the snake robot, presents experimental results that validate the function of the contact force measurement system, and demonstrates some of the motion capabilities of the robot.**

I. Introduction

Inspired by biological snake locomotion, snake robots carry the potential of meeting the growing need for robotic mobility in unknown and challenging environments. These mechanisms typically consist of serially connected modules capable of bending in one or more planes. The many degrees of freedom of snake robots provide traversability in irregular environments that surpasses the mobility of the more conventional wheeled, tracked and legged forms of robotic mobility.

The unique feature of snake robot locomotion compared to other forms of robotic mobility is that irregularities on the ground are actually beneficial for the propulsion since they provide push-points for the snake robot. While *obstacle avoidance* is an important topic for wheeled, tracked and legged robots, the goal of snake locomotion is rather *obstacle exploitation*. The term *obstacle-aided locomotion* was introduced by Transeth *et al.* [1] and captures the essence of this concept. Several empirical and analytical studies of biological snakes have been presented that shows the importance of external push-points on the locomotion of snakes [2]–[4].

A variety of snake robot designs have been developed so far. Hirose developed the world's first snake robot as early as 1972 [3]. This snake robot was equipped with passive wheels along its body. The use of passive wheels enables a snake robot to achieve propulsion on flat surfaces by propagating horizontal waves backwards along its body, and is a feature exploited by several other wheeled snake robots [5], [6]. Snake robots without wheels also exist [1], [7]–[11]. To the authors' best knowledge, the works in [1], [8] present the only published experimental results concerning obstacle-aided locomotion with wheel-less snake robots. Obstacle-aided locomotion with wheeled snake robots have been studied in [3], [12].

Affiliation of Pål Liljebäck is shared between the Department of Engineering Cybernetics at the Norwegian University of Science and Technology, NO-7491 Trondheim, Norway, and SINTEF ICT, Dept. of Applied Cybernetics, N-7465 Trondheim, Norway. E-mail: Pal.Liljeback@sintef.no

K. Y. Pettersen and Øyvind Stavdahl are with the Department of Engineering Cybernetics at the Norwegian University of Science and Technology, NO-7491 Trondheim, Norway. E-mail: {Kristin.Y.Pettersen, Oyvind.Stavdahl}@itk.ntnu.no

Fig. 1. The snake robot, Kulko.

This paper builds on the assumption that a snake robot needs two distinct features in order to successfully demonstrate obstacle-aided locomotion in an unknown and cluttered environment. These are characteristic features of biological snakes, but have received limited attention in snake robot designs so far. The first requirement is a *smooth exterior surface* along the body of the snake robot that will allow the snake to glide forward as a result of the external forces acting on the body. Any irregularities along the body will potentially obstruct the locomotion when the snake robot glides across an irregular surface. The second requirement is a *contact force sensing system*. Contact force sensing allows the robot to detect when the body is in contact with a push-point and also control the force exerted on a push-point. Since the sum of contact forces along the snake body is what propels the snake forward, the ability to measure these forces is important in order to control the propulsion.

This paper describes the development of a snake robot aimed at meeting both requirements listed above, i.e. a smooth exterior surface combined with a contact force sensing system. The paper details the design and implementation of the snake robot and presents experimental results that validate the function of the contact force measurement system. The motion capabilities of the robot are also demonstrated. We will not present experimental results on obstacle-aided locomotion both due to space restrictions and since the purpose of this paper is to describe the design of the snake robot. This paper extends previous work by the authors presented in [13], where the preliminary design of a single joint module of the snake robot was presented.

The paper is organized as follows. Section II gives a short overview of the snake robot design. Section III presents the actuation mechanism of the joint. Section IV describes how the smooth exterior surface of the snake robot is achieved. Section V describes the contact force measurement system. Section VI describes the control system of the joints. Section

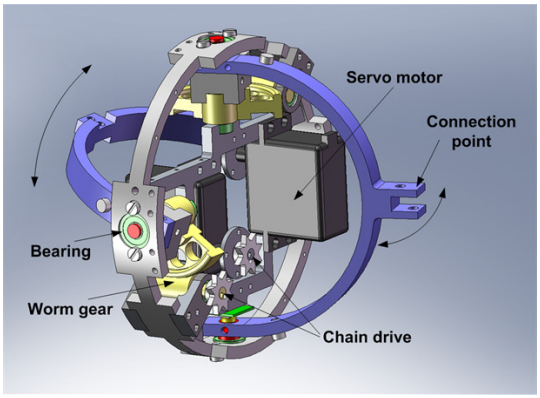

Fig. 2. Illustration of the articulation mechanism of the joint modules.

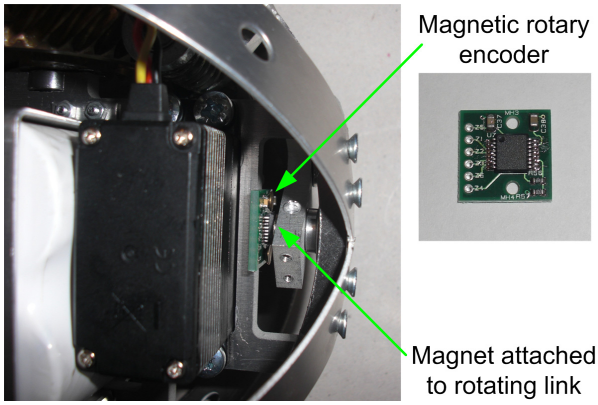

Fig. 3. Magnetic rotary encoder used for measuring the joint angle.

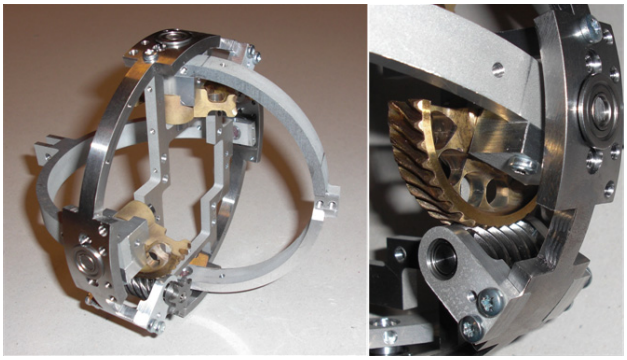

Fig. 4. The implemented articulation mechanism of the joint modules.

VII presents experimental results concerning the contact force measurement system and demonstrates the motion capabilities of the robot, and finally Section VIII presents concluding remarks.

II. Overview of the Snake Robot Design

As argued in the previous section, a snake robot needs a smooth exterior surface and a contact force sensing system in order to demonstrate intelligent obstacle-aided locomotion in unknown and cluttered environments. The snake robot presented in this paper has been developed to meet both these requirements. The idea is to encapsulate each joint module by a spherical shell that gives the joint a smooth outer surface no matter how the joint is flexed. Contact force sensing is achieved by mounting force sensors underneath the spherical shell, which enables the the snake robot to measure contact forces acting on the spherical surface. The complete snake robot, which is called *Kulko*, is shown in Fig. 1 and consists of a serial connection of identical ball-shaped joint modules. The various components of the snake robot are detailed in the following sections.

III. Joint Actuation Mechanism

As illustrated in Fig. 2, the articulation mechanism of each joint module has two degrees of freedom and consists of two links supported by bearings in a steel ring. The outer diameter of the steel ring is 130 mm. Each link has a connection point at its centre that allows it to be connected to the next joint module by two screws. The axes of rotation of the two links are orthogonal and intersecting.

The angle of the two moving links in the joint are measured with magnetic rotary encoders (AS5043 from austriamicrosystems). A magnet measuring 6 mm in diameter is attached to each link so that it rotates above the rotary encoder as shown in Fig. 3. Each encoder is attached to a custom-designed circuit board shown to the right in Fig. 3.

Each link is driven by a Hitec servo motor (HS-5955TG) by connecting the output shaft of each motor to a worm gear (gear ratio of 1:5.71) through a steel roller chain. The worm gear and the chain drive are shown in Fig. 4 and Fig. 5. The servo motors are manufactured to have a limited range of rotation (about $\pm 90°$). However, the gearing between the motors and the links requires the motors to rotate more than this limited range. The motors were therefore manually modified in order to enable them to rotate continuously. The process of modifying the servos is very simple and consists of disconnecting the output shaft of the servo from its internal potmeter and also removing a mechanical pin inside the servo that otherwise would prevent the servo from rotating continuously.

Worm gears have a disadvantage due to a high friction component in the gear system. However, worm gears are advantageous in that they may essentially produce any desired gear ratio in a single gear stage. This facilitates a compact design. In addition, a worm gear is not likely to break in contrast to e.g. spur gears. This makes the joint mechanically robust. The steel roller chain between the servo motor and

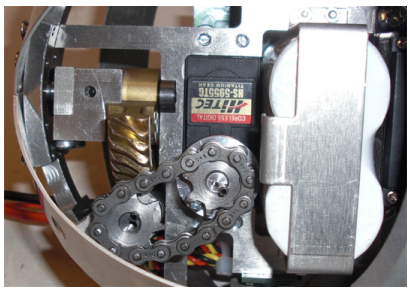

Fig. 5. Roller chain connecting the servo motor to the worm gear.

TABLE I

PARAMETERS OF THE ACTUATION MECHANISM.

Parameter	Value
Total weight of joint	960 g
Outer diameter	130 mm
Max joint travel	±45°
Max continuous joint torque	4.5 Nm
Max joint speed (no load)	$70°/_{\text{sec}}$

Fig. 6. Left: The upper and lower hemispherical shell of a joint module. Right: The smooth gliding surface along the snake robot.

the worm gear is rated to handle forces significantly higher than the forces produced by the servo motor.

Experiments indicate that the servo motors produce a maximum continuous torque of about 1.6 Nm (at 6V supply voltage with a maximum current drain of about 3A). The rated power efficiency of the worm gears is about 75 %. This should theoretically give the joint mechanism a maximum continuous torque of around 7 Nm. However, experiments with the implemented joint mechanism indicate that the maximum continuous torque lies around 4.5 Nm. This is probably due to more friction in the worm gear than expected and also some friction in the chain drive. Table I lists the parameters characterizing the actuation mechanism.

IV. EXTERIOR GLIDING SURFACE

Each joint module is covered by two hemispherical shells in order to give it a smooth outer surface. The shells and the resulting smooth gliding surface along the snake robot are shown in Fig. 6. A smooth surface is important to achieve gliding snake locomotion in irregular environments. Each hemispherical shell is 1.5 mm thick, weighs 42 g, and has an outer diameter of 140 mm. The shells were moulded from a plastic material.

As illustrated to the left in Fig. 7, four aluminium plates (indicated with a red colour) are bent around the joint in order to support the shells and also to allow for contact force measurements. Each shell is attached to the joint mechanism by two screws, as shown to the right in Fig. 7. The locations of the attachment screws define the *top* and *bottom* of the snake robot. The splice between the two hemispherical shells lies in the horizontal plane. The shells have a slit on each side corresponding to the range of motion of the connection points to the two neighbouring joints.

It is possible to achieve a more smooth exterior surface by installing a thin hollow cylinder of e.g. a plastic material between each joint module. This is illustrated in Fig. 8, but has not yet been implemented on the physical snake robot.

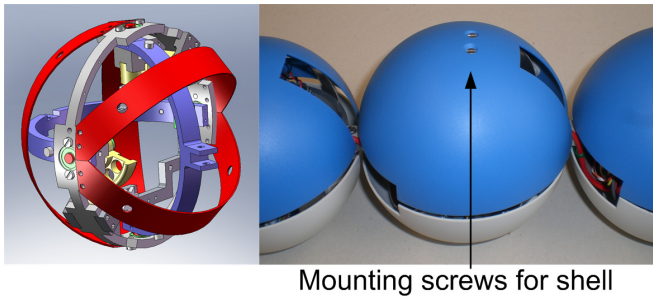

Fig. 7. Left: The four curved aluminium plates (with red colour) used for mounting force sensors. Right: The pair of screws attaching the shell to the joint mechanism.

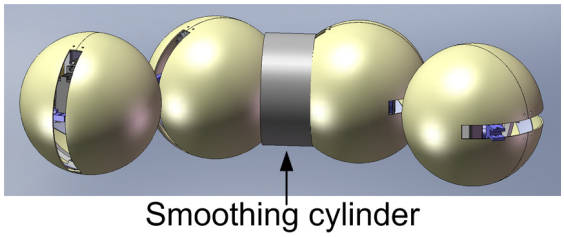

Fig. 8. Installing a thin cylinder between each joint module will further smoothen the exterior surface of the snake robot.

V. CONTACT FORCE MEASUREMENT SYSTEM

A. Assumptions underlying the sensor system

The purpose of the contact force measurement system is to enable the snake robot to conduct intelligent obstacle-aided locomotion, which requires the ability to detect contact forces along the snake body. The aim of the snake robot described in this paper is to demonstrate *obstacle-aided locomotion on horizontal surfaces*. The current design therefore assumes that all contact forces are applied at the sides of the joint and not at the top or bottom. This assumption affects the placement of the contact force sensors.

The contact force measurement system has been developed to provide information about *contact forces with respect to the macroscopic shape of the snake robot*. Information about the specific location of an applied contact force within a single joint module is not believed to be of significant interest during obstacle-aided locomotion since the location of a force within a single joint module only has a minor effect on the snake locomotion compared to the location of the force with respect to the entire snake robot. This means that the sensor system is *only required to determine the magnitude of a contact force and also at which side of a joint module it is applied*, but not the specific location where the force is applied on the outer shell. It should be noted that information about the force location within a joint module could be extracted from the force measurements by relating the magnitude of the measured forces to the relative placement of each sensor. Since the location of the contact force with respect to the shell is not determined by the sensor system, it will not be possible to determine the exact direction of the contact forces. However, the authors conjecture that it will be adequate to *approximate the direction of any*

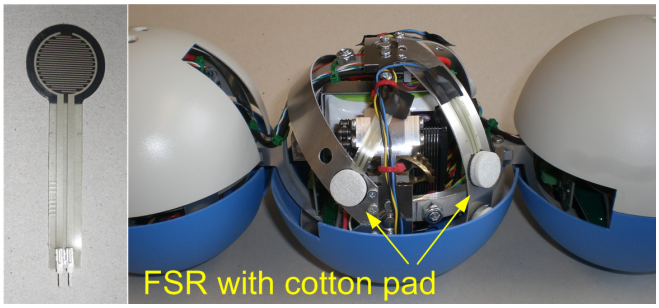

Fig. 9. Left: FSR (force sensing resistor) used to measure contact forces. Right: FSRs covered by cotton pads mounted to a joint module.

contact force as being normal to the macroscopic shape of the snake robot at the location where the force is applied.

B. The sensor system setup

A set of force sensing resistors (FSRs) are used to measure the external contact forces applied to each joint module. A FSR is a polymer thick film device that exhibits a decrease in electrical resistance when the force applied to the active surface area of the sensor increases. Due to effects such as hysteresis, a FSR is not suited for precision measurements. However, the authors conjecture that obstacle-aided locomotion with a snake robot does not require very precise force measurements. This, combined with its low cost and ease of use, makes FSRs suitable as a force sensor on snake robots. The use of FSRs on snake robots for contact force sensing have previously been attempted in [7], [11].

The FSR chosen for the snake robot has a diameter (active sensor area) of 13 mm and is shown to the left in Fig. 9. The right of Fig. 9 shows the placement of the FSRs on the curved aluminium plates covering each joint. A small cotton pad (3 mm thick) is placed over each FSR in order to distribute the applied force across the entire active area of the sensor. Four FSRs are placed at each side of a joint module in order to be able to measure horizontal contact forces, as explained in Section V-A. There are, in other words, eight FSRs mounted to each joint module. The exact placement of the FSRs around the joint is not critical since, as explained in the next section, the magnitude of the contact force is estimated by simply summing the contact forces measured by each FSR.

Note that the hemispherical shells enclosing the sensors are not completely rigid, i.e. the shells are, to some extent, deformable. This, combined with the deformability of the cotton pads placed over each FSR, means that there is compliance between the sensors and the location of an applied force. Compliance is necessary in order to measure the magnitude of the contact forces.

The controller board for the joint, which is described in Section VI, contains a set of identical voltage divider circuits for measuring the resistance through the FSRs. The circuit diagram for the voltage divider circuit is shown in Fig. 10. The voltage V_{ADC}, where ADC denotes *analog to digital converter*, is the FSR measurement signal and is given as a function of the variable resistance, R_{FSR}, across the FSR.

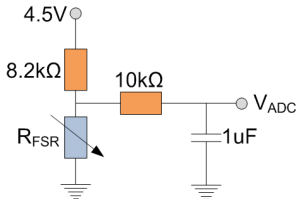

Fig. 10. Voltage divider circuit used to measure the resistance through the FSR.

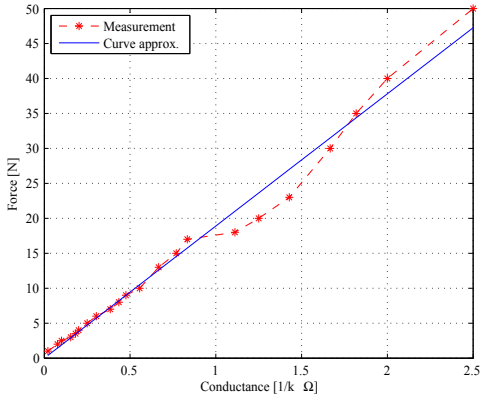

Fig. 11. The measured conductance (1/R) of the FSR as a function of applied force (measurements indicated by '*'). The solid line shows the linear curve approximation to these measurements.

C. Force measurement

The force vs. resistance characteristic of a FSR is extremely nonlinear. However, as shown in Fig. 11, there is a near linear relationship between the conductance (1/resistance) of a FSR and the force applied to it. The measurements in the figure are indicated by '*' and were conducted by placing an FSR on a digital scale. The scale was used to measure the force applied to the FSR while simultaneously measuring the electrical resistance through the FSR. A linear curve approximation to these measurements is plotted with a solid line in Fig. 11. The linear curve approximates the relationship between the force, F_{FSR}, applied to a FSR as a function of its conductance, G_{FSR}, and resistance, R_{FSR}. Based on the measurements, the expression for this linear curve was estimated as

$$F_{\text{FSR}} = 18.9 \cdot G_{\text{FSR}} = \frac{18.9}{R_{\text{FSR}}} \tag{1}$$

A simple mapping may now be derived between the FSR measurement voltage in Fig. 10, V_{ADC}, and the estimated applied force, F_{FSR}. The measurement voltage is given by

$$V_{\text{ADC}} = \frac{R_{\text{FSR}}}{R_{\text{FSR}} + 8.2} 4.5 \tag{2}$$

Solving (1) for R_{FSR}, inserting into (2), and solving for F_{FSR} give

$$F_{\text{FSR}} = \frac{4.5 - V_{\text{ADC}}}{8.2 V_{\text{ADC}}} 18.9 \tag{3}$$

As explained in Section V-B, each side of the joint mechanism is equipped with four FSRs. Since the spherical shell covering the joint mechanism is only in contact with

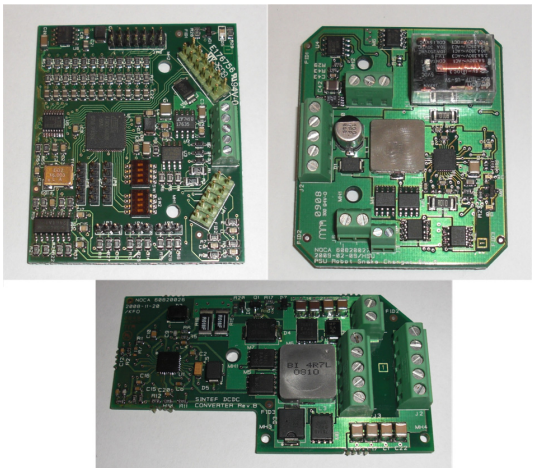

Fig. 12. The three custom-designed circuit boards located in each joint module. Top left: Microcontroller card that controls the joint mechanism. Top right: Battery charger card. Bottom: Motor power supply card.

the internal structure of the joint through the FSR measuring points, the magnitude of an external contact force applied to the joint may be estimated by simply summing the forces measured at each FSR. Note that the attachment of the shells causes the shells to induce a constant pressure on the force sensors even when there are no external forces acting on the shells. This produces a constant force offset that we subtract from the force measurements. The force offset is calculated as the average force during the first second after the snake robot is powered up. Denoting the four FSR measurements on the left side of the joint by $F_{\text{FSR,left},1}, .., F_{\text{FSR,left},4}$, the measurements on the right side of the joint by $F_{\text{FSR,right},1}, .., F_{\text{FSR,right},4}$, and the force offset on the left and right side of the joint by $F_{\text{left,offset}}$ and $F_{\text{right,offset}}$, respectively, the external forces, F_{left} and F_{right}, applied to the left and right side of the joint, respectively, are given by

$$\begin{aligned} F_{\text{left}} &= \left(\sum_{i=1}^{4} F_{\text{FSR,left},i}\right) - F_{\text{left,offset}} \\ F_{\text{right}} &= \left(\sum_{i=1}^{4} F_{\text{FSR,right},i}\right) - F_{\text{right,offset}} \end{aligned} \tag{4}$$

VI. Power and Control System

Motion control and supply of power to the components of each joint module are handled by three custom-designed circuit boards installed in each joint module. These circuit boards are shown in Fig. 12 and are described in the following subsections.

A. Power system

Fig. 13 illustrates the flow of power to the various components of a joint module. Each joint is powered by two serially connected Lithium Ion batteries from A123Systems of the type ANR26650M1. The batteries produce a supply voltage of about 6.6V at a capacity of 2.3Ah. The batteries were chosen due to their ability to deliver high currents (rated at 70A continuous discharge current) and also their short charge time (rated at 15 min charge time at 10A charge current).

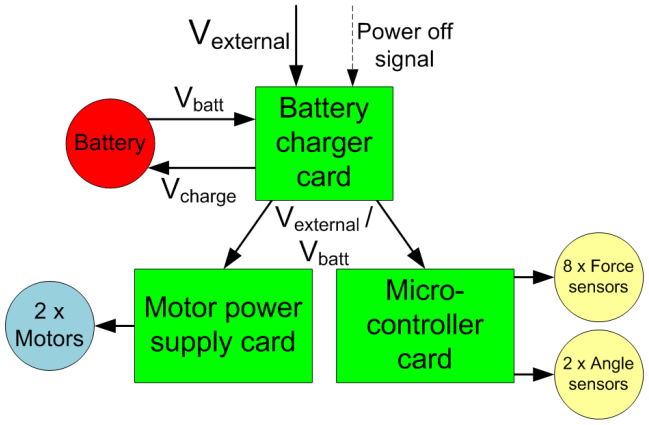

Fig. 13. Supply of power to the components of a joint module.

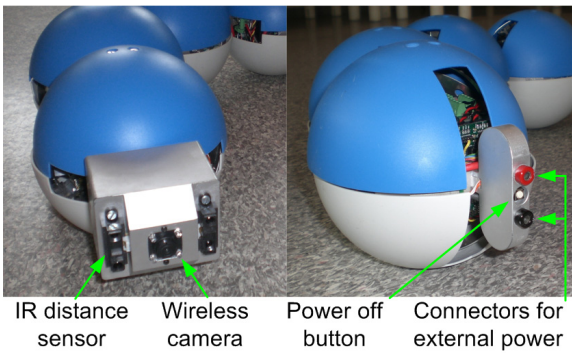

Fig. 14. Left: The head of the snake robot. Right: The tail of the snake robot.

Each battery is charged by an individual battery charger card shown to the top right in Fig. 12. The charging is automatically initiated by applying an external voltage to the external power connectors located at the tail of the snake robot (see the right of Fig. 14). Each battery is connected in series with a relay, which is controlled by a power off button also located at the tail of the snake robot.

The motor power supply card, shown at the bottom of Fig. 12, supplies power to the two servo motors driving each joint. This card converts the voltage supplied by the battery charger card to the motor voltage (6 V). The voltage supplied by the battery charger card is either the battery voltage (when external power is disconnected) or the external voltage (when external power is connected).

B. Control system

The data flow between the components of the snake robot is illustrated in Fig. 15. Motion control is handled by the microcontroller card shown to the top left in Fig. 12, which is based on the Atmel microcontroller AT90CAN128. This card continuously reads angular measurements from the two magnetic encoders (see Fig. 3) and also contact force sensor data from the FSRs (see Fig. 9). This card also generates PWM pulses for controlling the two servo motors driving the joint. The card has a CAN bus interface for communicating with the other modules of the snake robot.

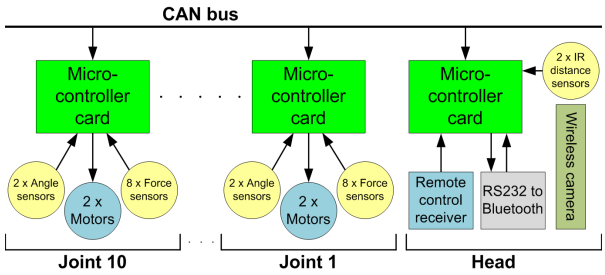

Fig. 15. The data flow between the modules of the snake robot.

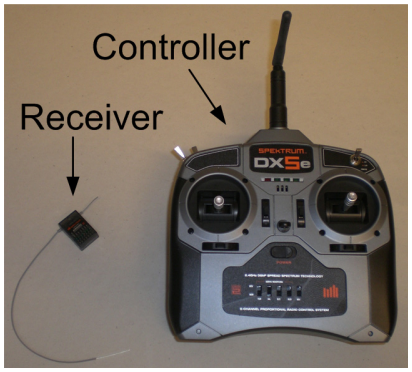

Fig. 16. The remote controller and the receiver used for controlling the snake robot.

The brain (or head) of the snake robot is shown to the left in Fig. 14. It contains the same microcontroller card that controls the motion of the joints. The brain card is responsible for sending joint reference angles to all joint modules over the CAN bus. The joint reference angles are calculated on an external computer in accordance with a defined control strategy and sent to the brain card via a wireless connection based on Bluetooth. We will not present control strategies for obstacle-aided locomotion in this paper. The authors have previously presented such a control strategy in [14].

For simple demonstration purposes (not for experimental purposes), the snake robot can also be manually controlled with a commercially available radio transmitter (the DX5e developed by Spektrum shown in Fig. 16). The receiver of the radio controller is connected to the brain card, which calculates joint reference angles based on the input from the radio controller. The mapping from radio control input to resulting joint reference angles will not be detailed here.

As shown to the left in Fig. 14, the head of the snake robot is equipped with a small wireless camera and two IR distance sensors (Sharp GP2D120). These sensors will be used to prevent the head from colliding with obstacles in its path.

VII. Performance of the Snake Robot

This section presents experimental results that validate the function of the contact force measurement system, and also shows the ability of the snake robot to display different motion patterns.

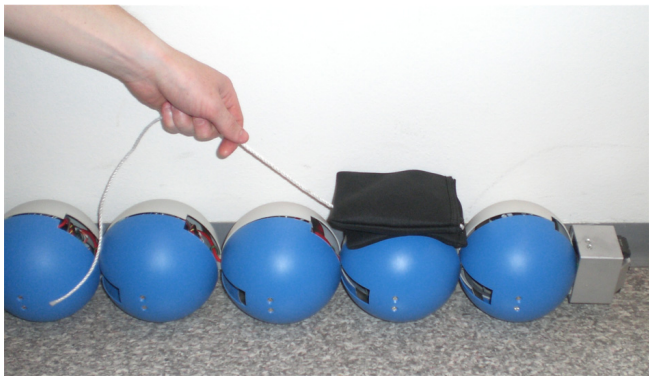

Fig. 17. The setup of the experiment conducted in order to test the contact force measurement system.

A. Experimental validation of the contact force measurement system

The setup of the experimental validation of the contact force measurement system is shown in Fig. 17. The snake robot was placed against a wall and flipped so that the left side of the robot was facing upwards. Loads with different weights were then dragged backwards along the part of the snake robot facing upwards (i.e. the left side) while each joint module measured the resulting contact forces. Each joint reported the measured forces over the CAN bus to the brain module, which redirected these measurements to an external computer over the wireless Bluetooth connection. The contact forces on the joint modules were calculated according to (4), and the measurements were sent to an external computer with a sampling frequency of 10 Hz.

Three different loads weighing 1350 g, 2750 g, and 4300 g, respectively, were dragged from the head and backwards along the snake robot. The resulting force measurements at joint 4, joint 5, and joint 6 (joint 1 is the foremost module) are shown in Fig. 18, Fig. 19, and Fig. 20, respectively. In theory, the amplitude of each force curve should be 13.5 N, 27.5 N, and 43 N, respectively, for the three different loads. Despite some deviations, the measured forces agree well with the weight of the loads. As described in Section V-B, a FSR is not suitable for precision measurements. Some deviations were therefore expected. The authors of this paper conjecture that obstacle-aided locomotion with a snake robot primarily requires the ability to detect a contact force and also, to some extent, assess the magnitude of this force. The experimental results indicate that the proposed sensor setup is able to meet these requirements.

Note that an ideal sensor system would produce a linear horizontal curve corresponding to the weight of the load being dragged along the snake body. Since the plots of the measured forces are instead given as peaks, it is clear that the sensor system does not measure forces *between* the joints very well. However, we do not consider this to be a critical issue in order to demonstrate obstacle-aided locomotion, especially not if the obstacles are large compared to the size of each joint module.

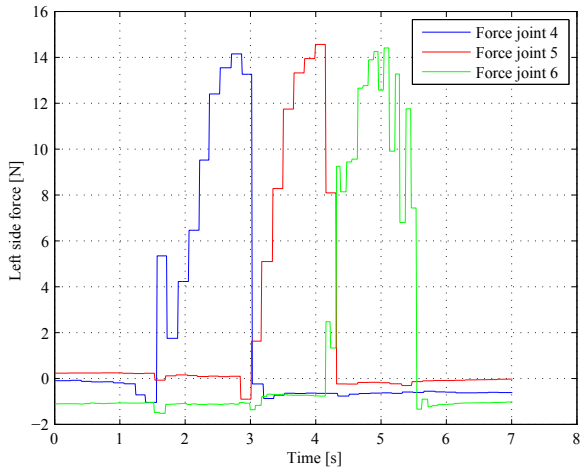

Fig. 18. Forces measured by joint 4 - 6 when a load weighing 1350 g was dragged along the snake robot.

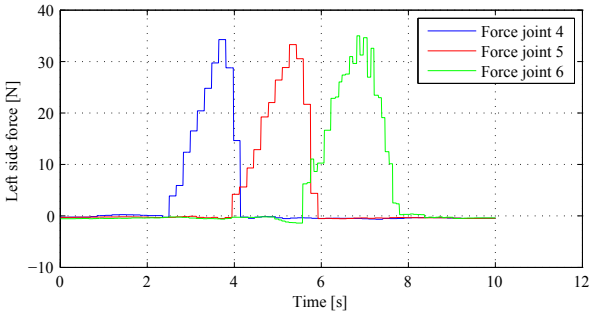

Fig. 19. Forces measured by joint 4 - 6 when a load weighing 2750 g was dragged along the snake robot.

B. Motion patterns

Some of the motion capabilities of the snake robot are demonstrated in Fig. 21 and Fig. 22, respectively. In Fig. 21 the snake robot conducts sidewinding across a flat surface. This is a sideways motion produced by propagating body waves backwards along the snake (see e.g. [15]). In Fig. 22 the snake robot conducts lateral rolling, which is a rolling motion produced by continuously creating a U-shape with the snake body that tips over to one side (see e.g. [5]).

In summary, the authors conjecture that the motion capabilities of the snake robot are satisfactory and adequate in order to demonstrate obstacle-aided locomotion.

VIII. Concluding Remarks

This paper has presented a new snake robot aimed at demonstrating intelligent obstacle-aided locomotion in cluttered and irregular environments. The snake robot was designed based on the assumption that obstacle-aided locomotion requires a snake robot to have a smooth exterior surface (in order to glide across irregular surfaces) combined with a contact force sensing system (in order to adapt to the environment). Both these features are incorporated in the proposed snake robot.

The paper has presented experimental results that validate the function of the contact force measurement system, and

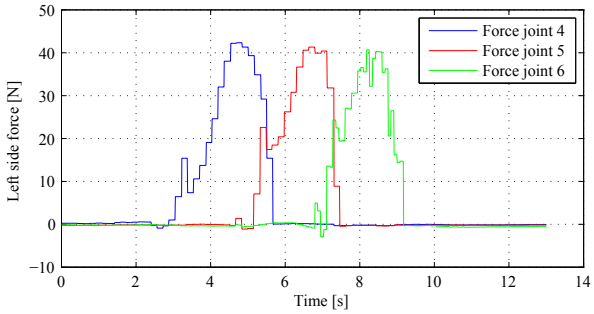

Fig. 20. Forces measured by joint 4 - 6 when a load weighing 4300 g was dragged along the snake robot.

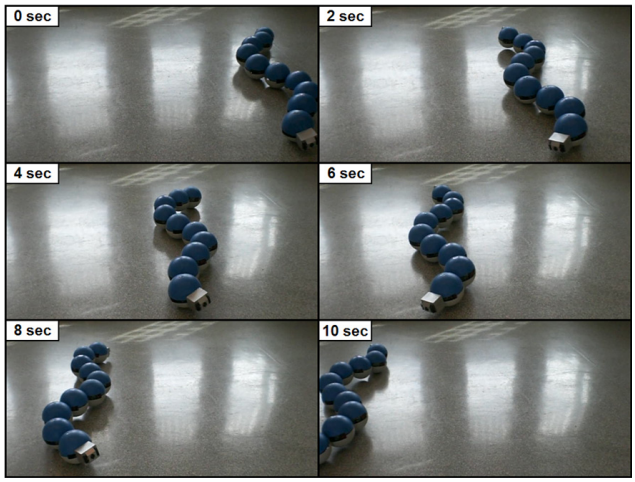

Fig. 21. The snake robot sidewinding across the floor.

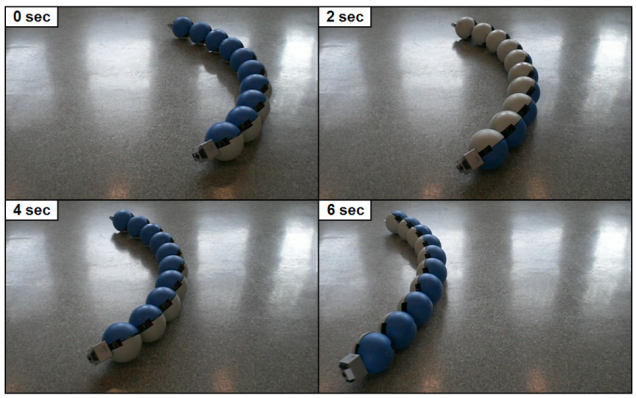

Fig. 22. The snake robot conducting lateral rolling across the floor.

also demonstrated some of the motion capabilities of the robot. Based on the successful demonstration of several motion patterns combined with the satisfactory performance of the contact force sensor system, the authors expect the proposed snake robot to be a suitable test-bed for investigating obstacle-aided locomotion in practice.

REFERENCES

[1] A. A. Transeth, R. I. Leine, C. Glocker, K. Y. Pettersen, and P. Liljebäck, "Snake robot obstacle aided locomotion: Modeling, simulations, and experiments," *IEEE Trans. Robot.*, vol. 24, no. 1, pp. 88–104, February 2008.

[2] J. Gray, "The mechanism of locomotion in snakes," *J. Exp. Biol.*, vol. 23, no. 2, pp. 101–120, 1946.

[3] S. Hirose, *Biologically Inspired Robots: Snake-Like Locomotors and Manipulators*. Oxford: Oxford University Press, 1993.

[4] B. Moon and C. Gans, "Kinematics, muscular activity and propulsion in gopher snakes," *Journal of Experimental Biology*, vol. 201, pp. 2669–2684, 1998.

[5] M. Mori and S. Hirose, "Three-dimensional serpentine motion and lateral rolling by active cord mechanism ACM-R3," in *Proc. IEEE/RSJ Int. Conf. Intelligent Robots and Systems*, 2002, pp. 829–834.

[6] H. Yamada, S. Chigisaki, M. Mori, K.Takita, K. Ogami, and S. Hirose, "Development of amphibious snake-like robot ACM-R5," in *Proc. 36th Int. Symp. Robotics*, 2005.

[7] P. Liljebäck, Ø. Stavdahl, and A. Beitnes, "SnakeFighter - development of a water hydraulic fire fighting snake robot," in *Proc. IEEE Int. Conf. Control, Automation, Robotics, and Vision*, Dec 2006.

[8] Z. Y. Bayraktaroglu, A. Kilicarslan, A. Kuzucu, V. Hugel, and P. Blazevic, "Design and control of biologically inspired wheel-less snake-like robot," in *Proc. IEEE/RAS-EMBS Int. Conf. Biomedical Robotics and Biomechatronics*, February 2006, pp. 1001–1006.

[9] H. B. Brown, M. Schwerin, E. Shammas, and H. Choset, "Design and control of a second-generation hyper-redundant mechanism," in *Proc. IEEE/RSJ Int. Conf. Intelligent Robots and Systems*, 2007, pp. 2603–2608.

[10] C. Wright, A. Johnson, A. Peck, Z. McCord, A. Naaktgeboren, P. Gianfortoni, M. Gonzalez-Rivero, R. Hatton, and H. Choset, "Design of a modular snake robot," in *Proc. IEEE/RSJ Int. Conf. Intelligent Robots and Systems*, 2007, pp. 2609–2614.

[11] S. A. Fjerdingen, J. R. Mathiassen, H. Schumann-Olsen, and E. Kyrkjebø, "Adaptive snake robot locomotion: A benchmarking facility for experiments," in *European Robotics Symposium 2008*, vol. 44, 2008, pp. 13 – 22.

[12] H. Date and Y. Takita, "Adaptive locomotion of a snake like robot based on curvature derivatives," in *Proc. IEEE/RSJ Int. Conf. Intelligent Robots and Systems*, San Diego, CA, USA, Oct-Nov 2007, pp. 3554–3559.

[13] P. Liljebäck, S. Fjerdingen, K. Y. Pettersen, and Ø. Stavdahl, "A snake robot joint mechanism with a contact force measurement system," in *Proc. IEEE Int. Conf. Robotics and Automation*, 2009, pp. 3815–3820.

[14] P. Liljebäck, K. Y. Pettersen, and Ø. Stavdahl, "Modelling and control of obstacle-aided snake robot locomotion based on jam resolution," in *Proc. IEEE Int. Conf. Robotics and Automation*, 2009, pp. 3807–3814.

[15] A. A. Transeth, R. I. Leine, C. Glocker, and K. Y. Pettersen, "3D snake robot motion: Non-smooth modeling, simulations, and experiments," *IEEE Trans. on Robotics*, vol. 24, no. 2, pp. 361–376, April 2008.